Advanced redox zonation of the San Pedro Sula alluvial aquifer (Honduras) using data fusion and multivariate geostatistics

Diego Di Curzio[1]*, Sergio Rusi[1], Patrizio Signanini[1]

[1]Department of Engineering and Geology (InGeo), University "G. d'Annunzio" of Chieti-Pescara, Via dei Vestini, 30 - 66013 Chieti, Italy.

Emails: sergio.rusi@unich.it; signanin@unich.it

*Corresponding author: diego.dicurzio@unich.it

Abstract

The incorrect wastewater management and the land use distribution lead to severe environmental problems, creating heavy eutrophication condition in surface-water. When surface-water/groundwater relationships exist, the organic matter transferred to the aquifer oxidizes and triggers redox processes (i.e. Terminal Electron Accepting Processes, TEAPs), such as Mn and Fe mobilization. This issue indeed provokes severe groundwater quality modifications, complicating its exploitation and management. For this reason, the definition of the redox zonation within an aquifer can be an effective tool for the identification of the contamination sources and for the conceptual model refinement, when remediation strategies need to be planned. Although the redox processes are dynamic reactions, the redox zonation is generally aimed to identify homogenous zones within an aquifer, characterized by a predominant TEAP. To overcome this methodological approach, the Multi-Collocated Factorial Kriging (MCFK) has been applied to physico-chemical parameters diagnostic of redox processes, that analyzes their spatial relationships at different scales.

The selected study area is the San Pedro Sula aquifer (north-western Honduras), which is a multi-layer alluvial aquifer characterized by well-known surface-water/groundwater

interactions and by heavy eutrophicated streams. Here, high concentrations of Mn and Fe were found in the aquifer.

The MCFK results show a short-range variability, highlighting a strong relation between Mn concentrations and anoxic conditions, due to the organic matter transfer from heavy polluted surface-water to the aquifer. Simultaneously, the relation between Fe and turbidity can be due to a fine colloidal phase, developed when different redox conditions of groundwater mix up in the wells. At a wider range, Fe seems to be related to redox processes, near the other contamination source detected in the northern San Pedro Sula alluvial plain. These results are supported by both the Principal Component Analysis and the hydrogeochemical numerical modeling. Ultimately, different TEAPs occur simultaneously in polluted areas, acting at multiple scales.

Keywords: redox processes; anoxic conditions; aquifer zonation; multivariate geostatistics; surface-water eutrophication; groundwater

1. Introduction

The redox processes are chemical reactions, that take place in groundwater via electron transfer (Marcus, 1956). These redox reactions, also known as Terminal Electron Acceptor Processes (TEAPs), are triggered by the organic matter present in the aquifer, either natural (e.g. peat) or anthropogenic (e.g. fuel-related compounds). This organic matter undergoes to hydrolysis and fermentation (McMahon and Chapelle, 1991; Jackson and McInerney, 2002; Watson et al., 2003; Heimann et al., 2010), that transform highly complex organic polymers into by-products, such as H_2, Acetate, and other short-chain fatty acids. These by-products represent the actual organic substrate (Electron Donor, ED). The organic substrate oxidation consumes other redox-sensitive compounds (Terminal Electron Acceptors, TEAs), such as O_2, NO_3^-, Mn(IV) and Fe(III) oxi-hydroxides,

SO_4^{2-} and dissolved inorganic carbon. TEAPs are generally microbially mediated and occur sequentially, depending on the required energy expressed in terms of Gibbs free energy (Berner, 1981; Postma and Jakobsen, 1996; Appelo and Postma, 2005; Rotiroti et al., 2018). The organic substrate degradation takes place by means of bacterial species, that consume energy for their growth and survival in a more or less efficient manner, according to the specific TEA used in the oxidation reaction (Hunter et al., 1998; Chapelle et al., 2002; Islam et al., 2004; Druschel et al., 2008; Lin et al., 2012). Thus, when organic substrate oxidizes in a particular aquifer, groundwater becomes enriched in reduced species of N, Mn, Fe, S and C that, in turn, trigger several secondary hydrogeochemical processes, such as mineral precipitation (e.g. Siderite, Rhodocrosite, Pyrite, etc.), pH variations, solid matrix changes and degassing (Christensen et al., 2000; Greskowiak et al., 2006; Molinari et al., 2014 Rotiroti et al., 2015). Furthermore, all these processes affect mobility, transport, degradation and toxicity of organic and inorganic contaminants (McCarty, 1997; Skubal et al., 1999; Sracek et al., 2004; Borch et al., 2010; Wallis et al., 2010; Barbieri et al., 2011; Rotiroti et al., 2014, Rusi et al., 2018).

For these reasons, the spatial distribution of redox processes within aquifers (i.e. redox zonation) is a topic of major interest. In literature, several studies can be found about the redox zonation of aquifers, that define homogeneous zones characterized by a well-defined TEAP. The parameters that are taken into account in these studies, as highlighted by Christensen et al. (2000), are multiple. The most widely used parameters are those related to the groundwater chemistry, with a particular focus on the inorganic TEA concentrations. From a methodological point of view, various approaches exist. McMahon and Chapelle (1991), Chapelle et al. (1996) and Chapelle et al. (2009a) defined redox zone distribution describing in detail the redox-sensitive compound and organic substrate distribution within aquifers. Kloppmann et al. (1996) and Postma and Jakobsen (1996) identified the predominant redox process by means of thermodynamic considerations. In

79 order to standardize the redox zonation of aquifers, McMahon and Chapelle (2008)
80 proposed TEA thresholds, that allowed to identify the predominant TEAP. This approach is
81 widely used in literature (Chapelle et al., 2009b; Landon et al., 2011; Close et al., 2016)
82 because it allows delineating a qualitative distribution of a specific redox process. Novel
83 approaches to the redox zonation consider multivariate statistics (Hsu et al., 2010;
84 Palmucci et al., 2016a, 2016b), that enables to study statistical relationships among
85 selected parameters, and the hydrogeochemical numerical modeling (Hunter et al., 1998;
86 Lønborg et al., 2006; Jakobsen and Cold, 2007; Boano et al., 2010). Studies that define
87 redox zones the organic substrate concentrations (i.e. H_2 and short-chain fatty acids), or
88 the bacterial species involved in TEAPs, are less common (Chapelle et al., 1996; Chapelle
89 et al., 2009b). The redox potential (Eh) is generally analyzed together with other physico-
90 chemical parameters because it does not describe a specific TEAP and its field
91 measurement is quite difficult and ambiguous (Christensen et al., 2000).
92 In all the previously described studies, the spatial relationships among the physico-
93 chemical parameters involved in redox processes are not considered, especially when the
94 electron acceptor type, distribution and amount are variable. For this reason, the main
95 objective of this research is to propose an up-to-date approach to the redox zonation of
96 aquifers using the Multi-Collocated Factorial Kriging (MCFK), a multivariate geostatistical
97 technique that allows analyzing the spatial relationships among the physico-chemical
98 parameters involved in redox processes. Since TEAPs are dynamic and reversible
99 reactions, that can take place even simultaneously, this methodological approach
100 overcomes the concept of homogeneous redox zones. The multivariate geostatistical
101 analysis is supported by the Principal Component Analysis (PCA) and the aqueous metal
102 speciation of Mn and Fe, performed by means of hydrogeochemical numerical modeling.
103 The selected case study (Fig.1) is the San Pedro Sula aquifer (Honduras), where
104 anomalous concentrations of Mn and Fe were detected, in some cases higher than the

thresholds suggested by the WHO (2011). Here, the urbanization and the agricultural, livestock and industrial activities strongly threatened the environmental quality and the groundwater management and exploitation for drinking and irrigation purposes (Madonna et al., 2007; Di Curzio et al., 2016).

Since the proposed methodological approach is very versatile and independent from local conditions, it could be implemented in other studies on redox zonation, regardless of the aquifer size, type, and location.

The proposed method was applied to data related to both the wet and dry seasons. In order to present the obtained result more clearly, all the results related to the dry season and other elaborations, useful to understand the environmental problem, are provided in the Supplementary Material file.

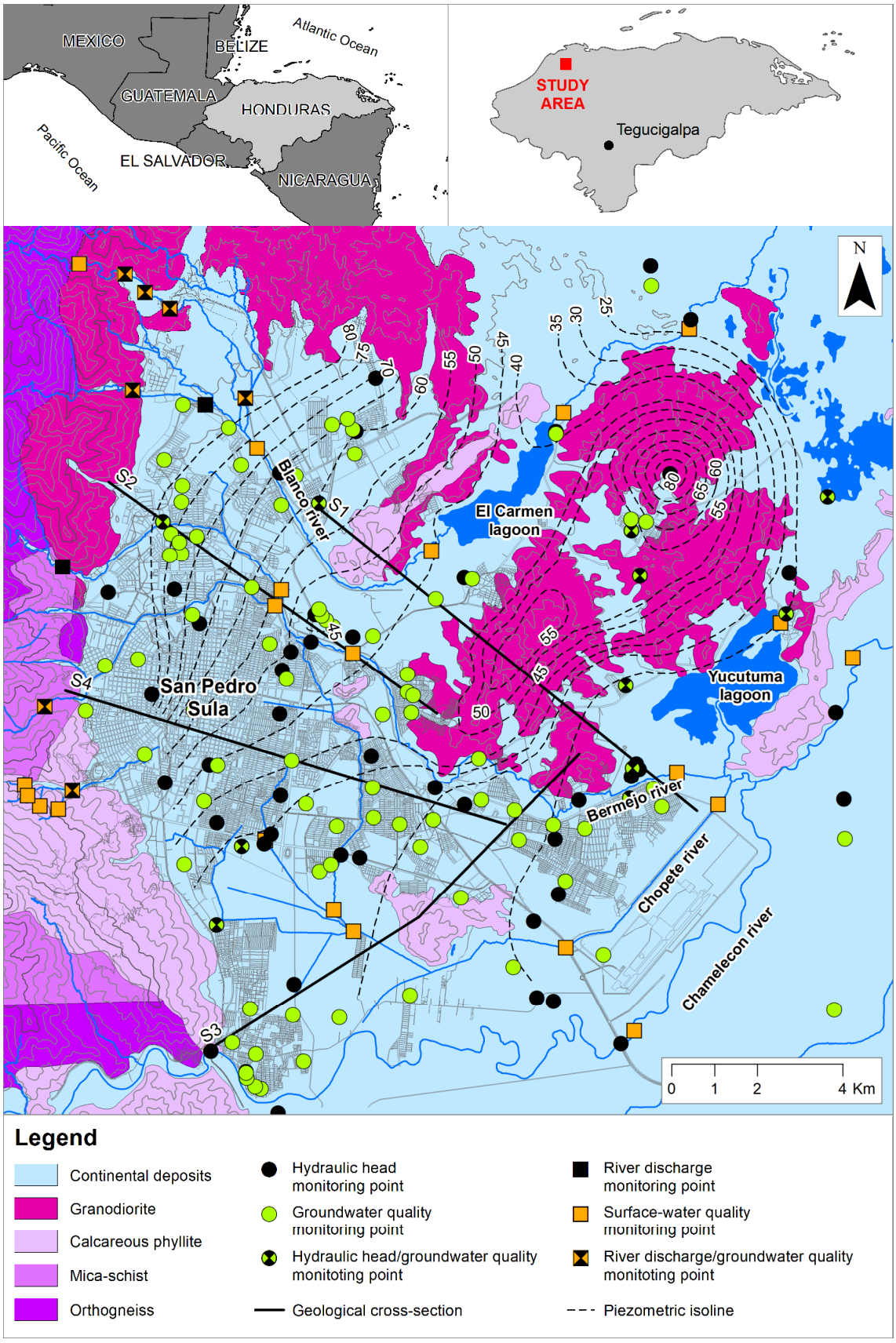

Fig. 1. The hydrogeological map of the San Pedro Sula plain, with the monitoring network and the geological cross-section traces shown in Fig. 2.

2. Material and methods

2.1. Study area

The San Pedro Sula alluvial plane, in Honduras (Central America), is the northern part of the Sula Valley and hosts an extended urban area. It is a tectonic depression, whose origin is related to the strike-slip fault system of the margin between the North-American and the Caribbean plates (Donnelly et al, 1990; Aldrich et al, 1991; Rogers et al, 2007; Garza et al, 2012; Capaccioni et al, 2014).

In the study area (Fig. 1), Paleozoic-Precambrian metamorphic rocks, characterized by different metamorphic grade (i.e. Orthogneiss, mica-schists, Calcareous Phyllite), constitute the bedrock. In the eastern part of the San Pedro Sula plain, a granodioritic batholite is present (Cretaceous-Tertiary), bounded by hydrothermal sulfide minerals (Finch, 1981; Torrese et al., 2006; Madonna et al., 2007; Torrese et al., 2013), that appears morphologically as a hill. All the lithotypes that compose the bedrock are highly weathered and fractured. The tectonic depression is filled up by continental deposits. As previously seen in similar geological contexts (Vessia and Di Curzio, 2018; Di Curzio et al., 2018), the filling continental deposits are highly heterogeneous, characterized by complex geometries, and more than hundreds meter thick (Fig. 2). These deposits consist of sandy gravels (i.e. slope-alluvial deposits) near the valley slopes, and silty sands and clayey silts (i.e. alluvial-lacustrine deposits) in the central part of the plain. At shallow depth, sandy gravelly paleo-channels were detected near the main streams (Madonna et al., 2007; Torrese et al., 2013).

These heterogeneous continental deposits and, to a lesser extent, the weathered and fractured bedrock represent the San Pedro Sula aquifer. In detail, this is a multi-layer aquifer, characterized by medium to high permeability silty sandy and sandy gravelly layers interdigitated with low permeability clayey silty layers (Torrese et al., 2006; Madonna et al., 2007; Torrese et al., 2013).

146 The hydraulic head analysis (Fig. 1) suggests that the recharge areas are located in the
147 north-western part, near the valley slopes, and eastern part, in correspondence of the
148 granodioritic hill, of the study area. Groundwater flow takes place within the porous
149 continental deposits and, to a lesser extent, within the weathered and fractured bedrock,
150 mainly toward the Chamalecon river, although it has a radial component in
151 correspondence of the granodioritic hill toward the El Carmen Lagoon, the Yucutuma
152 Lagoon, and the north-eastern wetlands. These lagoons and wetlands are groundwater
153 dependent because the aquifer thickness decreases in this area and the water emerges
154 on the surface (see cross-section S1 in Fig. 2). Surface-water/groundwater relationships
155 are evident even for some parts of the main streams (i.e. Blanco river, Bermejo river,
156 Chopete river, in Fig. 1), especially in the eastern part of the urban area, related to the
157 shallow sandy gravelly paleo-channels.
158 The rainfall difference (about 200 mm) between the wet (February) and dry season (April)
159 affects both the stream discharge (Tab. SMX in Supplementary Material) and the hydraulic
160 heads (Fig. 1).
161 The land use distribution in San Pedro Sula plain (Fig. SMX in Supplementary Material),
162 carried out by the Direccion de Investigacion y Estadistica Municipal of San Pedro Sula in
163 2004, shows 3 predominant areas: 1) the large urban and industrial area, 2) the wide area
164 dedicated to livestock in the northern part the plain, and 3) the intensive agricultural area
165 near the Chamalecon river. The agricultural, livestock and industrial activities represent
166 potential contamination sources, that can likely affect the surface-water and groundwater
167 environmental quality (Wang et al., 2011; Meneses et al., 2015).
168

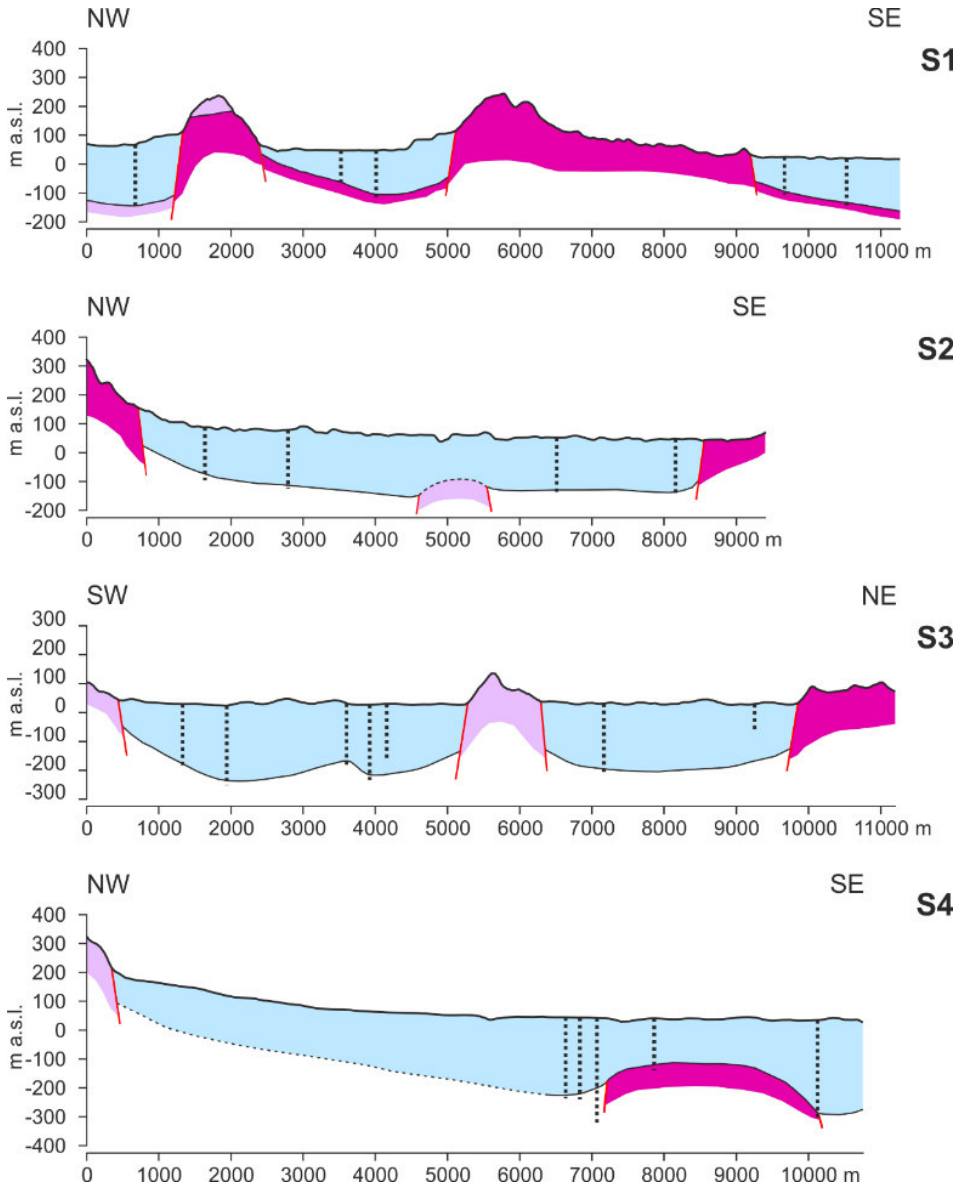

Fig. 2. Geological cross-section of the San Pedro Sula plain (vertical exaggeration 4x). The vertical dotted lines represent the geognostic surveys.

2.2. Dataset

The data used in this study were provided by the water management organization of San Pedro Sula (i.e. Agua de San Pedro Spa). In detail, physico-chemical data related to 2 monitoring rounds were considered: February (wet season) and April (dry season) 2002. The monitoring network, represented in Fig. 2, consists of 93 wells and 32 surface-water sampling points. Al the monitored wells show a completion characterized by gravel package for the whole borehole length and filters in correspondence of the more

permeable aquifer layers. In some of the sampling points, either the stream discharge or the hydraulic head were measured.

The chemical analyses of both surface-water and groundwater samples, previously filtered (d=0.45 μm), include the physico-chemical parameters displayed in Tab. 1 and were performed following the Standard Methods for the Examination of Water and Wastewater (APHA-AWWA, 1998). For all the analyses, the chemical balance error resulted < 10%. In addition, the concentrations below the detection limit (DL) were considered as equal to $DL/2$.

In order to evaluate the groundwater contamination, the thresholds suggested by the WHO (2011) were considered.

Tab. 1. The analyzed parameters and the corresponding methods used for both surface-water and groundwater (APHA-AWWA, 1998).

Parameter	Method	Detection Limit	Description	Sample
T	2550 B	0.1° C	Laboratory measurement	Groundwater/Surface-water
pH	4500-H B	0.01	Potentiometric method	Groundwater/Surface-water
EC	2510 B	1 μS/cm	Potentiometric method	Groundwater/Surface-water
Turbidity	2130 B	0.01 NTU	Nephelometric method	Groundwater/Surface-water
Na^+	3500-Na D	0.1 mg/L	ICP/MS method	Groundwater/Surface-water
K^+	3500-K D	0.1 mg/L	ICP/MS method	Groundwater/Surface-water
Ca^{2+}	3500-Ca D	0.1 mg/L	EDTA titrimetric method	Groundwater/Surface-water
Mg^{2+}	3500-Mg D	0.1 mg/L	ICP/MS method	Groundwater/Surface-water
HCO_3^-	2320 B	1 mg/L	Titration method	Groundwater/Surface-water
Cl^-	4500-Cl B	0.1 mg/L	Iodometric method	Groundwater/Surface-water
SO_4^{2-}	4500-SO4 E	0.01 mg/L	Turbidimetric method	Groundwater/Surface-water
NO_3^-	4500-NO3 E	0.001 mg/L	Cadmium reduction method	Groundwater/Surface-water
NH_4^+	4500-NH3 C	0.001 mg/L	Titrimetric method	Groundwater/Surface-water
PO_4^{3-}	4500-P E	0.001 mg/L	Ascorbic acid method	Groundwater/Surface-water
Fe	3500-Fe D	0.01 mg/L	Phenanthroline method	Groundwater/Surface-water
Mn	3500-Mn D	0.01 mg/L	Persulfate method	Groundwater/Surface-water
DO	4500-O G	0.1 mg/L	Membrane electrode method	Surface-water
BOD_5	5210 B	0.01 mg/L	5-day BOD test	Surface-water
COD	5220 B	0.01 mg/L	Open reflux method	Surface-water

196 *2.3. Principal Component Analysis*

197 The Principal Component Analysis (PCA) is a multivariate statistical technique, that allows
198 identifying relations within a data matrix $n \times N$ related to some selected parameters ($z_i(\mathbf{x})$).
199 The fundamental principle of this method is to combine the selected parameters values,
200 reducing the original data dimensionality and identifying new grouping variables, called
201 factors, or Principal Components (PCs). The PC extraction is performed by the following
202 matrix equation (Wackernagel, 2003):

203 $$\mathbf{Y} = \mathbf{ZQ}$$

204 where $\mathbf{Y}$ is a matrix $n \times N$ containing n of the Principal Components Y_p (with $p = 1, \dots, N$),
205 which are not correlated and with mean zero, $\mathbf{Z}$ matrix $n \times N$ of experimental data from
206 which the PCs are extracted, and $\mathbf{Q}$ is the eigenvector matrix of the Principal Components
207 Y_p.

208 For each Principal Component, correlation coefficients are defined, called loadings, that
209 represents the weight of each original variable of the PCs. The equation that defines the
210 correlation matrix is:

211 $$\mathbf{R} = \mathbf{Q\Lambda Q}^T = \left(\mathbf{Q}\sqrt{\mathbf{\Lambda}}\right)\left(\mathbf{Q}\sqrt{\mathbf{\Lambda}}\right)^T = \mathbf{AA}^T$$

212 where $\mathbf{\Lambda}$ is the diagonal matrix of eigen values, and $\mathbf{A}$ is the matrix of transformation
213 coefficients. These coefficients correspond to the covariances between the original
214 variables ($z_i(\mathbf{x})$) and the Principal Components Y_p.

215 In this manner, the relationships among the selected input parameters can be identified,
216 that allow describing statistically the physical processes involved. The loading values vary
217 from -1 and 1 and are given by the weight (score) that each data has on a specific PC. In
218 order to maximize the variance of squared loadings and to improve the PC interpretation,
219 the Varimax method was selected (Palmucci and Rusi, 2014; Viaroli et al., 2016).

220 Each identified PC explains a percentage of the whole dataset variance. Therefore, the
221 more the variance percentage is large, the more the processes explained by the PC is

222 important and predominant. To select the significative PCs, the Kaiser criterion was
223 selected, which considers only PCs with eigenvalue > 1 (Hotelling, 1933).
224 In this study, the PCA was chosen as an explorative statistical technique, in order to
225 identify the statistical relationships among the available physico-chemical parameters
226 (Tab. 1).
227
228 *2.4. Aqueous metal speciation*
229 The aqueous redox-sensitive metal species (e.g. Mn, Fe, As, Cr, etc.) distribution in
230 groundwater, depends on site-specific physico-chemical factors, such as pH, redox
231 condition, temperature, and dissolved ions (Kotas and Stasicka, 2000; Halim et al., 2005;
232 Reeder et al., 2006; Balistrieri et al., 2007; Root et al., 2009; Nedrich et al., 2018).
233 The redox equilibria in aqueous solutions, such as the metal speciation, are described by
234 the Nernst equation. This equation defines the redox potential (Eh, in Volt), related to a
235 specific redox reaction, as follows:
236 $$\mathrm{Eh} = \mathrm{E}^0 + \frac{\mathrm{RT}}{\mathrm{nF}} \ln \frac{[\mathrm{ox}]^{\mathrm{a}}}{[\mathrm{red}]^{\mathrm{b}}}$$
237 where E^0 is the standard potential (at 25° C and 1 atm), at which all the ions have activity
238 equal to one, R is the gas constant (equal to 8.314 J/mol K), T is the absolute temperature
239 (in K), n is the number of electrons transferred in the redox reaction, F is the Faraday
240 constant (96.42 kJ/Volt per gram equivalent), $[\mathrm{ox}]$ and $[\mathrm{red}]$ are respectively the oxidized
241 and reduced species, and a and b the corresponding stoichiometric coefficients.
242 These redox equilibria depend on the electron activity ($\mathrm{pe} = -\log[\mathrm{e}^-]$), that is defined from
243 the Nernst equation, as follows:
244 $$\mathrm{pe} = \frac{\mathrm{EhF}}{2.303\mathrm{RT}} = \frac{\mathrm{Eh}}{0.059}$$
245 The hydrogeochemical modeling of the metal speciation (PHREEQC, Appelo and Postma,
246 2005) allows identifying the distribution of redox-sensitive metal species in a particular

aqueous system. In detail, known the water chemistry and the pH and pe values, all the oxidized and reduced species of a specific redox-sensitive metal can be quantified. In the absence of direct Eh measurements, as in this study, the redox condition can be simulated by the activity ratio of other redox-sensitive compounds, such as NO_3^-/NH_4^+. Although this is clearly a simplification, this approach can reproduce reliably the redox condition of the considered aqueous solution.

In this study, the Mn and Fe speciations were performed, because their concentrations often exceeded the thresholds suggested by the WHO (2011).

2.5. Multivariate geostatistics

The multivariate geostatistical techniques considered in this study are based on the Linear Model of Coregionalization (LMC), that comprises direct variograms and cross-variograms (Wackernagel, 2003). In geostatistics, the variogram is the spatial dependency function of a given random function Z, considering a separation vector, known as lag ($\mathbf{h}$). In detail, the variance is defined as a function of di $\mathbf{h}$ (Webster & Oliver, 2007; Castrignanò, 2011; Chilès & Delfiner, 2012). In the multivariate case, the cross-variogram ($\gamma_{z_i,z_j}(\mathbf{h})$) represents a measurement of the joint variability of two variables $z_i(\mathbf{x}_\alpha)$ e $z_j(\mathbf{x}_\alpha)$ and is defined by the following equation:

$$\gamma_{z_i,z_j}(\mathbf{h}) = \frac{1}{2N(\mathbf{h})}\sum_{\alpha=1}^{N(\mathbf{h})}\{[z_i(\mathbf{x}_\alpha) - z_i(\mathbf{x}_\alpha+\mathbf{h})]\left[z_j(\mathbf{x}_\alpha) - z_j(\mathbf{x}_\alpha+\mathbf{h})\right]\} \quad \text{with } \alpha = 1,\dots,N(\mathbf{h})$$

where x_α is the location of the sampling point. According to the LMC, all the considered variables are considered as a result of the same independent processes, that occur at different scales. For this reason, the LMC is selected starting from the experimental direct variograms and cross-variograms, related to the considered variables. The $n(n+1)/2$ experimental direct variograms and cross-variograms are modeled as a linear combination of N_S basic variogram functions $g^u(\mathbf{h})$:

$$\gamma_{ij}(\mathbf{h}) = \sum_{u=1}^{N_S} b_{ij}^{u}\, g^{u}(\mathbf{h}) \quad \text{with } i, j = 1, \dots, n$$

where $\gamma_{ij}(\mathbf{h})$ are the variogram models, u is the spatial scale and b_{ij}^{u} are the partial sill of the spatial structure $g^{u}(\mathbf{h})$, that describes each contribution to the whole dataset variance. Using the matrix notation, the previous equation becomes:

$$\boldsymbol{\Gamma}(\mathbf{h}) = \sum_{u=1}^{N_S} \mathbf{B}^{u}\, g^{u}(\mathbf{h})$$

where $\boldsymbol{\Gamma}(\mathbf{h})$ is $n \times n$ matrix, whose diagonal elements are the direct variograms, while the non-diagonal elements are the cross-variograms, and $\mathbf{B}^{u}$ is a symmetric matrix of the LMC coefficients b_{ij}^{u}, called Coregionalization Matrix.

If the LMC comprises also secondary auxiliary variables, continuous in the whole domain (i.e. the interpolation grid), the multivariate geostatistical methods will become Multi-Collocated. This approach decreases considerably the computation time and improves the primary variable estimation and the definition of their spatial relationships (Andrade and Stigter, 2013; Castrignanò et al., 2012, 2015).

The Multi-Collocated Co-Kriging (MCCK) is a multivariate technique that improves the estimation of primary variables, by the following linear estimator ($z_{i_0}^{*}(\mathbf{x}_0)$):

$$z_{i_0}^{*}(\boldsymbol{x}_0) = \sum_{i=1}^{n} \sum_{\alpha=1}^{n_i} \lambda_{\alpha}^{i}\, z_i(\boldsymbol{x}_\alpha) \quad \text{with } i = 1, \dots, n$$

where $\mathbf{x}_0$ is the position where the variable is estimated and $z_i(\mathbf{x}_\alpha)$ are the measured values in the $\mathbf{x}_0$ neighborhood.

By imposing the optimal unbiased estimation condition, the MCCK system of equations can be obtained. This system consists in $\sum_{i=1}^{n} n_i + n$ linear equations and $\sum_{i=1}^{n} n_i + n$ variables, represented by the weights λ_{β}^{j} and n Lagrangian coefficients μ_i:

293
$$\begin{cases} \sum_{j=1}^{n}\sum_{\beta=1}^{n_j}\lambda_\beta^j\gamma_{ij}(\mathbf{x}_\alpha,\mathbf{x}_\beta)+\mu_i=\gamma_{ii_0}(\mathbf{x}_\alpha,\mathbf{x}_0) \quad \text{with } i=1,\dots,n \text{ and } \alpha=1,\dots,n_i \\ \sum_{\beta=1}^{n_i}\lambda_\beta^i=\delta_{ii_0} \quad \text{with } i=1,\dots,n \end{cases}$$

294 where δ_{ii_0} is the Kronecker delta, that is 1 or 0 in case of primary or auxiliary variables
295 respectively. The estimation uncertainty is measured by the variance ($\sigma^2(\mathbf{x}_0)$), that is
296 obtained by the following equation:

297
$$\sigma^2(\mathbf{x}_0)=2\sum_{i=1}^{n}\sum_{\alpha=1}^{n_i}\lambda_\alpha^i\,\gamma_{ii_0}(\mathbf{x}_\alpha,\mathbf{x}_0)-\sum_{i=1}^{n}\sum_{j=1}^{n}\sum_{\alpha=1}^{n_i}\sum_{\beta=1}^{n_j}\lambda_\alpha^i\lambda_\beta^j\gamma_{ij}(\mathbf{x}_\alpha,\mathbf{x}_\beta)-\gamma_{i_0i_0}(\mathbf{x}_0,\mathbf{x}_0)$$

298 The Multi-Collocated Factorial Kriging (MCFK) is a multivariate geostatistical technique
299 that allows identifying the spatial relationships among the considered variables. This
300 method derives from the Factorial Kriging Analysis (FKA), proposed by Matheron (1982),
301 that is based on the regionalized PCA (Sollitto et al., 2010; Castrignanò et al., 2012, 2015;
302 Du et al., 2017). In detail, the Coregionalization Matrix (B^u), for each spatial scale u, is
303 decomposed into the eigenvalue and eigenvector matrices (Wackernagel, 2003).
304 Considering the PCA equations already defined in Section 2.3, the MCFK matrix equation
305 can be obtained:

306
$$\mathbf{B}^u=\mathbf{Q}^u\boldsymbol{\Lambda}^u\mathbf{Q}^{uT}=\left(\mathbf{Q}^u\sqrt{\boldsymbol{\Lambda}^u}\right)\left(\mathbf{Q}^u\sqrt{\boldsymbol{\Lambda}^u}\right)^T=\mathbf{A}^u\mathbf{A}^{uT}$$

307 where $\mathbf{Q}^u$ is the eigenvector matrix containing the regionalized factors $Y_v^u(\mathbf{x})$, $\boldsymbol{\Lambda}^u$ is the
308 eigenvalue diagonal matrix for each spatial scale u, and $\mathbf{A}^u$ is the matrix of transformation
309 coefficients a_{iv}^u, that represent the covariance values between the original variables $z_i(\mathbf{x})$
310 and the factors $Y_v^u(\mathbf{x})$. This approach, that allows identifying spatial factors reciprocally
311 orthogonal for each scale described by correlation coefficients with the original variables
312 (Wackernagel, 2003; Webster and Oliver, 2007; Castrignanò, 2011), is defined as follows:

313
$$z_i(\mathbf{x})=\sum_{u=1}^{N_S}\sum_{v=1}^{n}a_{iv}^u\,Y_v^u(\mathbf{x})$$

The obtained regionalized factors $Y_v^u(\mathbf{x})$ can be plotted as maps, providing an effective representation of spatial relationships among the considered variables.

Since the selected multivariate geostatistical methods are based on the hypothesis stationarity of 1st and 2nd order (Webster and Oliver, 2007), they can be applied only on Gaussian distributed datasets. For this reason, the considered variables were transformed by the Gaussian Anamorphosis, that converts a Gaussian variable Y into a new variable with any distribution $Z = \Phi(Y)$. This transformation is carried out by fitting a polynomial expansion (Chilès and Delfiner, 2012):

$$\Phi(Y) = \sum \Psi_i H_i(Y)$$

where $H_i(Y)$ are the Hermite polynomials and Ψ_i are their coefficients. To transform a non-Gaussian variable into a Gaussian one and to apply the selected multivariate methods, the Gaussian Anamorphosis function must be inverted:

$$Y = \Phi - 1(Z)$$

The Gaussian Anamorphosis function avoids bias when the LMC is selected.

In this study, the variables considered in the multivariate geostatistical methods are redox-related physico-chemical parameters (i.e. Fe, Mn, NH_4^+, NO_3^-, PO_4^{3-}, T, Turbidity, pH). Since surface-water/groundwater relationships were detected, the distance from surface-water (Dist in Fig. SMX) was selected as an auxiliary variable because TEAPs were considered to take place near the eutrophicated streams and lagoons.

All the multivariate geostatistical analyses were performed by means of ISATIS (Geovariances, 2017).

3. Results and discussion

3.1. Data description and basic statistics

Statistics of groundwater analyses are shown in Tab. 2. The electrical conductivity (EC) and the major ions (Na^+, K^+, Ca^{2+}, Mg^{2+}, HCO_3^-, Cl^-, SO_4^{2-}) are characterized by a very

high variability, as highlighted by the differences between the maximum and minimum values and the interquartile ranges, likely related to the duration of the water/rock interactions (Buss et al, 2008; Desiderio et al, 2010; Purcell et al, 2015; Ryan et al, 2015). The hydrogeochemical classification was carried out by means of the Ludwig-Langelier diagram (Fig. SM2 in Supplementary Material) and allowed identifying the different water-types of the San Pedro Sula aquifer. The water-type varies from Ca-HCO_3 to Na-HCO_3. Na-rich Ca-HCO_3 types occur frequently, especially when EC values are low. Since these water-types are typical of salt-water intrusion (Cary et al., 2015) and the study area is located far from the coastline, the Na-rich water-type causes were investigated by means of log-log diagrams of molar ratios among some major ions (i.e. HCO_3^-/Na^+ vs. Ca^{2+}/Na^+ and Mg^{2+}/Na^+ vs. Ca^{2+}/Na^+), to get a deeper insight into the water/rock interaction processes (Gaillardet et al., 1999; Dessert et al., 2003). For all the groundwater samples, the predominant process is the silicate dissolution (Fig. SM3 in Supplementary Material). In fact, these minerals constitute the aquifer solid matrix through which groundwater flows.

The water temperature increases from the recharge areas to the discharge ones, varying from values similar to the air temperature (17.0° C) to values typical of the San Pedro Sula aquifer (maximum value 25.0° C). The pH values, except few slightly acid samples (minimum value 5.58), are mainly alkaline (mean 7.31 and median 7.38). These pH values are typical of these water-types. The turbidity values, even though the samples were filtered, are variable, with a high maximum value (125.00 NTU). The redox-related parameters show similar statistical distribution. In detail, the NO_3^-, NH_4^+, and PO_4^{3-} concentrations are generally low in the aquifer, as shown by the mean (0.543 mg/L, 0.150 mg/L, and 0.146 mg/L, respectively) and median (0.075 mg/L, 0.076 mg/L, and 0.111 mg/L, respectively) values and by the corresponding interquartile ranges. Nevertheless, the maximum concentrations are considerably higher than the mean and median values (6.894 mg/L, 2.945 mg/L, and 0.815 mg/L, respectively). Furthermore, Mn and Fe show

366 the same statistical distribution, with low mean (0.16 mg/L and 0.23 mg/L, respectively)
367 and median (0.01 mg/L and 0.08 mg/L, respectively) values and very high maximum
368 concentrations (1.28 mg/L and 2.39 mg/L, respectively), that are significantly above the
369 thresholds suggested by the WHO (2011). Localized anoxic conditions can account for
370 these anomalous Mn and Fe statistical distributions.
371 Analyzing the Skewness (S) and Kurtosis (K) values, all the physico-chemical parameters
372 show a statistical distribution different from the Gaussian one (i.e. S = 0 e K = 3).
373
374 *Tab. 2. Descriptive statistics of groundwater physico-chemical parameters.*

	Unit	Count	Mean	Median	Min	Max	Q1	Q3	S	K
T	° C	93	21.8	22.0	15.0	25.0	20.0	23.0	-0.344	-0.013
pH		93	7.31	7.38	5.58	8.22	7.06	7.61	-0.948	2.260
EC	µS/cm	93	416	331	102	1312	206	527	1.252	0.842
Turbidity	NTU	93	5.49	0.20	0.01	125.00	0.15	1.00	4.609	21.501
Na^+	mg/L	93	30.4	20.9	6.8	125.4	16.5	37.9	1.901	3.969
K^+	mg/L	93	2.1	2.0	0.3	5.1	1.5	2.6	0.759	0.918
Ca^{2+}	mg/L	93	38.5	29.5	5.6	147.2	17.1	52.8	1.500	2.506
Mg^{2+}	mg/L	93	14.7	11.0	0.2	69.6	5.6	19.6	1.725	3.602
HCO_3^-	mg/L	93	186	156	11	451	101	249	0.893	-0.283
Cl^-	mg/L	93	21.3	12.5	0.5	102.7	7.2	25.0	1.884	2.902
SO_4^{2-}	mg/L	93	27.90	24.00	2.00	142.00	11.00	36.00	1.975	5.976
NO_3^-	mg/L	93	0.543	0.075	0.000	6.894	0.038	0.480	3.597	14.007
NH_4^+	mg/L	93	0.150	0.076	0.000	2.945	0.000	0.147	6.880	57.325
$PO4^{3-}$	mg/L	93	0.146	0.111	0.010	0.815	0.057	0.210	2.272	8.249
Fe	mg/L	93	0.23	0.08	0.00	2.39	0.04	0.19	3.495	13.100
Mn	mg/L	93	0.16	0.01	0.01	1.28	0.01	0.14	2.208	4.122

375
376 Beside physico-chemical parameter values related to the water/rock interaction (i.e. major
377 ions, pH and EC) similar to the groundwater ones, statistics of surface-water (Tab. 3)
378 highlight high values of some compounds (i.e. NH_4^+ e PO_4^{3-}) and indexes (i.e. BOD_5 e
379 COD). In addition, the dissolved oxygen (DO) content in surface-water is often below the
380 detection limit (i.e. 0.1 mg/L). These parameters represent the nutrient load and the
381 oxygen consumption in biological and chemical processes occurring in surface-water.
382 Heavy eutrophication conditions can account for these parameter values (Lee et al, 2015).

As for groundwater, the S and K values indicate non-Gaussian statistical distributions.

Tab. 3. Descriptive statistics of surface-water physico-chemical parameters.

	Unit	Count	Mean	Median	Min	Max	Q1	Q3	S	K
T	° C	32	20.8	21.0	18.0	25.0	20.0	22.0	0.082	1.218
pH		32	7.40	7.50	4.42	7.87	7.34	7.65	-4.519	23.155
EC	µS/cm	32	287	197	37	1370	83	363	2.145	6.280
Turbidity	NTU	32	16.85	15.00	0.20	70.00	3.00	25.00	1.478	2.218
Na	mg/L	32	25.1	11.0	4.2	244.5	6.7	29.2	4.618	23.750
K	mg/L	32	4.1	2.9	0.0	15.5	1.2	5.3	1.448	1.577
Ca	mg/L	32	19.2	14.8	2.0	51.2	6.4	30.0	0.789	-0.615
Mg	mg/L	32	7.3	6.2	0.5	54.7	1.2	9.1	3.818	18.008
HCO_3	mg/L	32	104	68	3	324	23	166	0.831	-0.536
Cl	mg/L	32	12.2	6.0	1.4	42.7	3.4	17.1	1.339	0.764
SO_4	mg/L	32	37.19	24.50	0.50	370.00	10.00	42.50	4.727	24.766
NO_3	mg/L	32	0.051	0.045	0.005	0.268	0.027	0.057	3.225	13.467
NH_4	mg/L	32	2.969	0.271	0.000	22.786	0.000	2.877	2.449	5.758
PO_4	mg/L	32	1.056	0.382	0.018	7.330	0.193	0.844	2.578	6.877
Fe	mg/L	32	0.75	0.45	0.05	3.96	0.18	1.12	2.241	7.165
Mn	mg/L	32	0.07	0.05	0.00	0.40	0.01	0.11	2.127	6.239
DO	mg/L	32	4.8	6.7	0.0	8.9	0.0	8.6	-0.243	-1.918
BOD_5	mg/L	32	53.75	4.85	0.20	350.00	1.10	105.00	1.899	3.714
COD	mg/L	32	98.34	23.25	1.00	474.00	9.20	185.00	1.482	1.593

3.2. Surface-water and groundwater quality

The distribution in the study area of the parameters indicating surface-water eutrophication (Fig. 3) identify low nutrient concentrations and BOD_5 e COD values on the slopes of the San Pedro Sula basin, sometimes below the detection limits. In these areas, the DO concentrations are high, attaining the natural values (i.e. oxygen saturation in water). This evidence indicates fair environmental conditions and complete absence of eutrophication. Contrariwise, in the streams flowing near the urban area (i.e. Bermejo river, Chopete river, in Fig. 1), the nutrient load is high as well as the BOD_5 e COD values, while the DO concentrations are always below the detection limit. These values indicate heavy eutrophication conditions and poor surface-water quality (Lewandowski et al., 2015; Meinikmann et al., 2015). The eutrophication conditions, in turn, create an organic matter surplus in surface-water. In the San Pedro Sula plain, the surface-water quality

399 deterioration likely depends on the incorrect wastewater management, that discharge
400 untreated in the main streams (i.e. Bermejo river, Chopete river, in Fig. 1). An additional
401 nutrient load can leach from the areas where the agricultural and livestock activities are
402 prevalent (Fig. SMX in Supplementary Material).

403

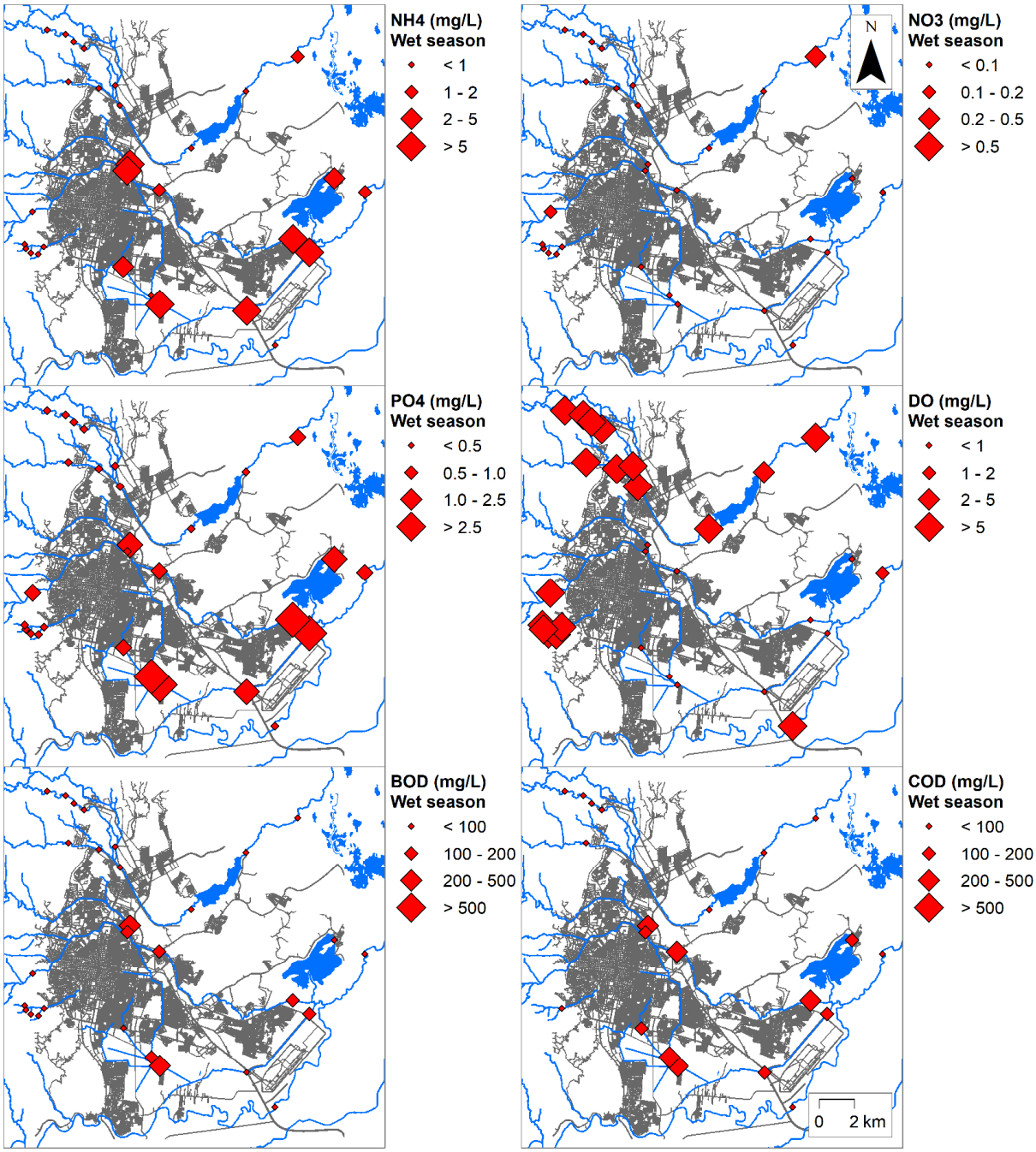

404
405 *Fig. 3. Eutrophication parameters and indexes distribution in surface-water.*

406

407 The Mn and Fe distribution in groundwater (Fig. 4) was obtained by the MCCK analysis.
408 The selected LMC is characterized by an isotropic nested structure (Chilès and Delfiner,
409 2012), consisting of a short-range spherical structure (range = 2300 m) and a long-range
410 spherical structure (range = 6000 m). The interpolation grid has 30x30 m cell size.
411 The MCCK results show that the worst surface-water quality is reflected in the Mn and Fe
412 distribution (Fig. 4). As a matter of fact, their concentrations are very high, far above the
413 WHO thresholds (0.1 mg/L and 0.3 mg/L, respectively for Mn and Fe), near the heavily
414 eutrophicated streams (i.e. Bermejo river and Chopete river) and lagoons (i.e. El Carmen
415 lagoon and Yucutuma lagoon). Furthermore, the same high Mn and Fe contents exist in
416 the northern area, where the San Pedro Sula industrial district is present. In this case, one
417 or multiple organic contamination events can account for these anomalous concentrations.
418

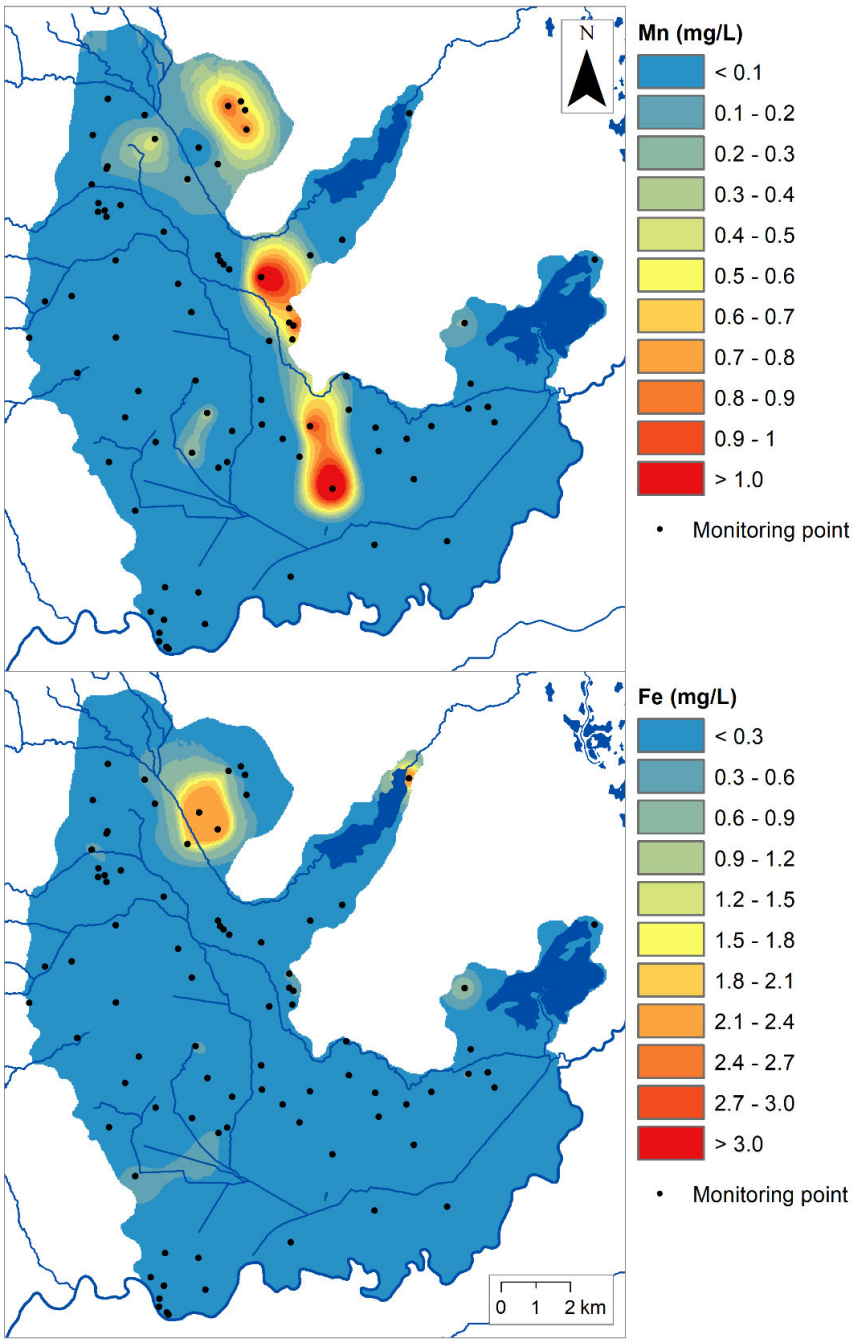

Fig. 4. Mn (upper part) and Fe (lower part) distributions in the San Pedro Sula aquifer.

3.3. Relations among groundwater physico-chemical parameters

The PCA (Fig. 5; Tab. 4 and 5) was performed considering all the available physico-chemical parameters.

The correlation matrix obtained by the PCA (Tab. 4) shows highly significative correlations concerning the major ions and the EC. Among others, the significant correlations between

427 Mn and NH_4^+ (r = 0.46), between Fe and turbidity (r = 0.33), and between e Fe and PO_4^{3-} (r
428 = 0.36) have to be emphasized.
429 Furthermore, the PCA identifies 3 PCs (Fig. 5; Tab. 5), describing 59.61% of the total
430 variance. In detail, the PC1 is highly correlated to the major ions and the EC. This principal
431 component describes the water/rock interaction processes, that cause an increase in total
432 dissolved solids. As already highlighted in Section 3.1, the groundwater chemistry of the
433 San Pedro Sula aquifer depends on the silicate dissolution process. The PC2 shows a
434 positive correlation with Mn (r = 0.67) and NH_4^+ (r = 0.71) and a negative correlation with
435 NO_3^- (r = -0.56). In this case, the TEAPs occurrence in groundwater, that leads to anoxic
436 conditions, is described. The anoxic conditions inhibit the NH_4 oxidation to NO_3^- and favor
437 the reductive dissolution of Mn(IV) oxi-hydroxides. Nevertheless, for N species,
438 denitrification cannot be completely excluded. In this hydrogeological framework, the
439 eutrophicated surface-water/groundwater relationships, that cause organic matter leaching
440 in the aquifer, and the organic contamination in the northern areas can trigger the TEAPs.
441 The PC3 is characterized by positive correlations with both Fe (r = 0.66) and turbidity (r =
442 0.79). This particular relation is likely related to mixed redox conditions that occur in the
443 monitoring wells because of their completion (see Section 2.2). The mixing of different
444 groundwater, characterized by very different redox conditions, can cause the TEAP
445 regression and Fe(III) oxi-hydroxide precipitation as a colloidal phase.
446

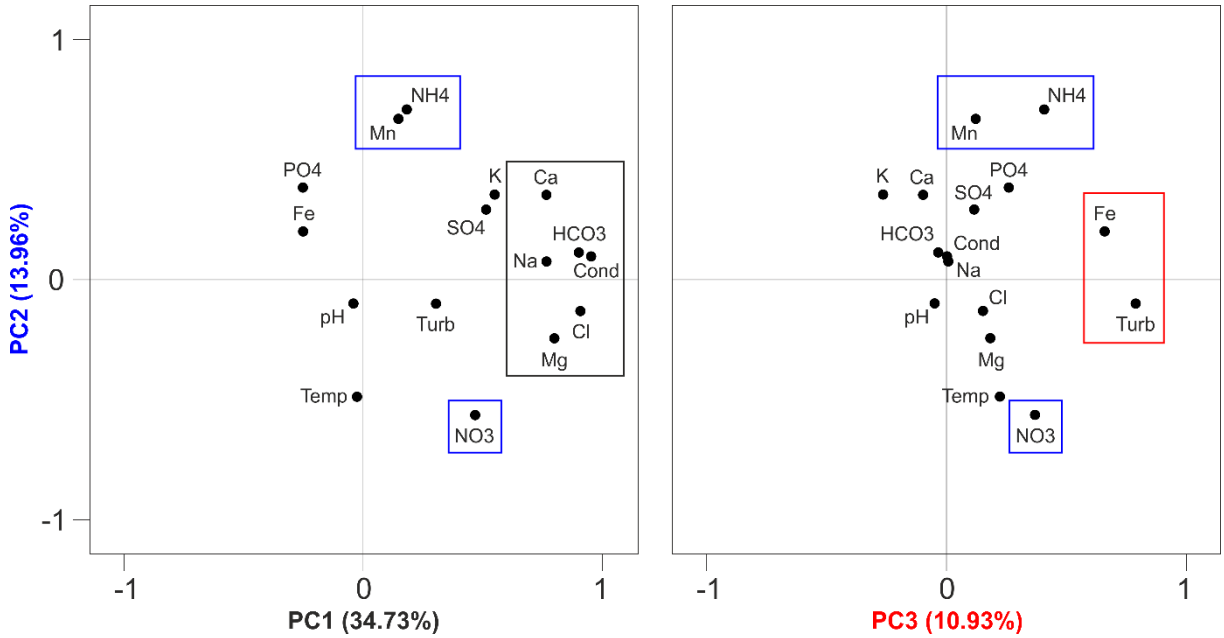

Fig. 5. Projection of the PC loadings obtained by the PCA. The percentage of variance described by each PC is given in brackets.

Tab. 4. Pearson correlation matrix of the analyzed physico-chemical parameters. The highly significative correlations are represented in underlined bold red, while the significative ones in underlined bold black. The significativity level was assessed by the Student's t-test.

	T	EC	pH	Turb	Na^+	K^+	Ca^{2+}	Mg^{2+}	HCO_3^-	Cl^-	SO_4^{2-}	NO_3^-	NH_4^+	PO_4^{3-}	Fe	Mn
T	1															
Cond	-0.10	1														
pH	0.14	0.08	1													
Turb	0.08	0.26	-0.07	1												
Na^+	-0.02	**0.74**	-0.03	0.20	1											
K^+	-0.16	**0.46**	-0.24	0.04	**0.41**	1										
Ca^{2+}	-0.13	**0.83**	0.16	0.11	**0.41**	**0.48**	1									
Mg^{2+}	0.11	**0.74**	0.07	**0.37**	**0.46**	0.19	**0.54**	1								
HCO_3^-	-0.03	**0.94**	0.15	0.21	**0.68**	**0.42**	**0.83**	**0.78**	1							
Cl^-	0.05	**0.85**	-0.09	**0.38**	**0.74**	**0.42**	**0.60**	**0.72**	**0.74**	1						
SO_4^{2-}	-0.11	**0.52**	0.04	0.24	**0.31**	0.28	**0.60**	**0.34**	**0.37**	**0.38**	1					
NO_3^-	0.23	**0.34**	-0.07	**0.40**	0.25	-0.01	0.08	**0.55**	0.26	**0.54**	0.17	1				
NH_4^+	-0.17	0.23	-0.08	0.28	0.12	0.27	**0.39**	0.05	0.25	0.10	0.27	-0.06	1			
PO_4^{3-}	-0.08	-0.22	-0.23	-0.07	-0.05	-0.03	-0.23	-0.23	-0.19	-0.16	-0.21	-0.16	0.26	1		
Fe	-0.04	-0.18	-0.19	**0.33**	-0.06	-0.13	-0.24	-0.20	-0.23	-0.07	-0.12	-0.10	0.18	**0.36**	1	
Mn	-0.15	0.12	-0.16	0.00	0.28	0.20	0.19	0.04	0.17	0.09	0.20	-0.19	**0.46**	0.27	0.11	1

Tab. 5. The rotated matrix of principal components, with the corresponding percentages of described variance. The significative correlations are represented in underlined bold red.

	PC1	PC2	PC3
T	-0.03	-0.49	0.22
pH	-0.04	-0.10	-0.05
Cond	**0.95**	0.10	0.00
Turb	0.30	-0.10	**0.79**
Na^+	**0.77**	0.08	0.01
K^+	**0.55**	0.35	-0.26
Ca^{2+}	**0.77**	0.35	-0.10
Mg^{2+}	**0.80**	-0.24	0.18
HCO_3^-	**0.90**	0.11	-0.03
Cl^-	**0.91**	-0.13	0.15
SO_4^{2-}	**0.51**	0.29	0.12
NO_3^-	0.47	**-0.56**	0.37
NH_4^+	0.18	**0.71**	0.41
PO_4^{3-}	-0.25	0.38	0.26
Fe	-0.25	0.20	**0.66**
Mn	0.15	**0.67**	0.12
Eig. Val.	5.56	2.23	1.75
Var. %	34.73	13.96	10.93

3.4. Mn and Fe aqueous speciation

The Mn and Fe speciation related to the groundwater samples was performed by the hydrogeochemical modeling, using the Wateq4f.dat thermodynamic database (Ball and Nordstrom, 2001).

The obtained results confirm the PCA ones. In detail, the Mn content in groundwater is completely correlated (R^2 = 0.99) with the reduced species of Mn (i.e. log[Mn^{2+}]), pointing out the clear dependency of the total Mn on the redox conditions (Fig. 6a). Concerning Fe, the modeling results show a good correlation between its total content in groundwater and the activity of its reduced form log[Fe^{2+}] (R^2 = 0.68), hence a certain dependency on the redox conditions exists (Fig. 6b). Nevertheless, some samples, whose turbidity is greater than 1, are characterized by total Fe concentrations above the ones that they should have at the corresponding redox conditions. For these cases, the modeled Ferrihydrite amounts were compared with the corresponding turbidity values (Fig. 6c). The good correlation (R^2 = 0.59) confirms the presence of Fe oxi-hydroxide colloidal phase, whose size is smaller

than the filter diameter. The two anomalies, represented in Fig 6c, can be attributable to colloidal phases, not related to the Fe content.

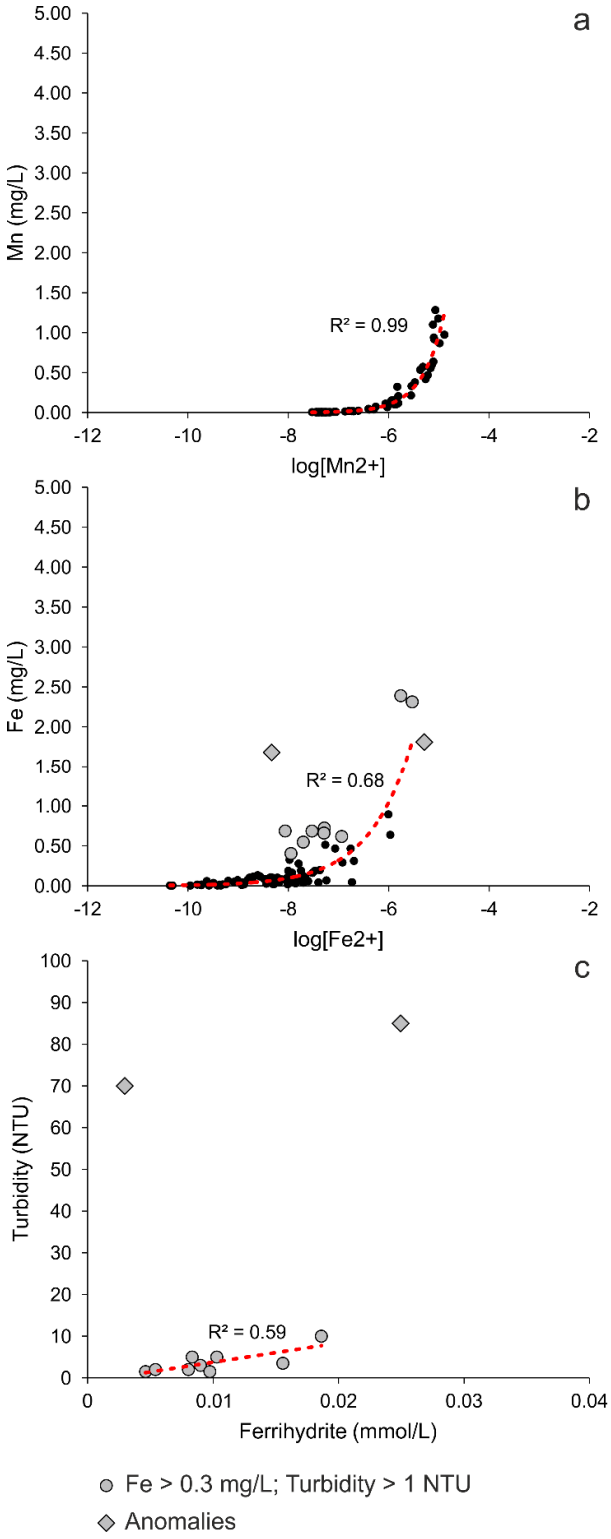

Fig. 6. Correlation between the activity of the reduced form of both Mn (a) and Fe (b) and their total content in groundwater. For the samples characterized by turbidity greater than 1, the modeled Ferrihydrite amounts were correlated with the corresponding turbidity values (c).

3.5. Advanced redox zonation

The application of the Multi-Collocated Factorial Kriging allowed to point out the spatial scale-dependent relationships among the redox-related physico-chemical parameters, already identified by the PCA and Mn and Fe speciation, and to perform the San Pedro Sula aquifer advanced redox zonation (Fig. 7).

The selected LMC, including both direct variograms and cross-variograms, is characterized by a nested model. This model consists of a spherical structure at short range (2300 m) and a spherical structure at long range (6000 m), explaining the variability at different scales. The short-range spherical structure (Tab. 6 and 7; Fig. 7a) individuates a regionalized factor describing 53.65% of the total variance at a smaller scale, while the long-range spherical structure (Tab. 6 and 8; Fig. 7b) individuates a regionalized factor describing 46.99% of the total variance at a wider scale.

The short-range factor is positively correlated with Fe, Mn, NH_4^+, and turbidity and negatively correlated with the groundwater temperature (Tab. 6). Furthermore, the corresponding structural correlation matrix (Tab. 7) indicates a high correlation between Fe and turbidity (r = 0.827). The small-scale relationships are the same as those pointed out by the PCA (i.e. PC2 and PC3) and the metal speciation. These results indicate the occurrence of anoxic conditions in groundwater and the simultaneous Fe oxi-hydroxide precipitation as a colloidal phase. Analyzing the spatial distribution of this short-range factor (Fig. 7a), these simultaneous redox processes take place near the eutrophicated streams and in the northern area, likely polluted organic compounds.

At long range (Tab. 6 e 8; Fig. 7b), the obtained factor is characterized by a positive correlation with Fe and PO_4^{3-} and a negative correlation with NO_3^-, indicating the exclusive Fe dependency on anoxic conditions. Furthermore, this factor demonstrates that anoxic conditions persist at a longer distance. This interpretation of the long-range factor even account for the high negative correlation between Fe and NO_3^- (r = -0.922), pointed out by

507 the structural correlation matrix (Tab. 8). The area affected by this long-range factor (with
508 scores > 1) is the northern one (Fig. 7b), where organic contamination was detected.

509

510 *Tab. 6. Decomposition into regionalized factors obtained by the MCFK. application to the selected Gaussian*
511 *variables (indicated with "g"). The significative correlations are represented in underlined bold red.*

	gFe	gMn	gNH4	gNO3	gPO4	gTemp	gTurb	gpH	gDist	Eig. Val.	Var. %
Spherical structure - Short Range (2300 m)											
F1	**0.378**	**0.371**	**0.557**	-0.215	0.210	**-0.358**	**0.410**	-0.135	-0.061	2.157	53.65
Spherical structure - Long Range (6000 m)											
F1	**0.537**	0.253	0.098	**-0.557**	**0.337**	-0.262	-0.213	-0.256	0.185	1.230	46.99

512

513 *Tab. 7. Structural correlation matrix at short range. The significative correlations are represented in*
514 *underlined bold black.*

	gFe	gMn	gNH4	gNO3	gPO4	gT	gTurb	gpH	gDist
gFe	1								
gMn	0.261	1							
gNH4	**0.575**	**0.460**	1						
gNO3	-0.206	**-0.485**	**-0.698**	1					
gPO4	0.051	0.268	**0.762**	**-0.690**	1				
gT	-0.185	**-0.428**	**-0.755**	**0.960**	**-0.773**	1			
gTurb	**0.827**	**0.573**	**0.684**	**-0.495**	0.095	**-0.438**	1		
gpH	-0.269	**-0.796**	-0.251	**0.581**	-0.127	**0.390**	**-0.519**	1	
gDist	**-0.381**	0.074	0.056	0.174	0.116	0.222	-0.170	0.091	1

515

516 *Tab. 8. Structural correlation matrix at long range. The significative correlations are represented in*
517 *underlined bold red.*

	gFe	gMn	gNH4	gNO3	gPO4	gT	gTurb	gpH	gDist
gFe	1								
gMn	0.198	1							
gNH4	**0.699**	**-0.448**	1						
gNO3	**-0.922**	**-0.472**	**-0.532**	1					
gPO4	**0.705**	**0.378**	**0.312**	**-0.593**	1				
gT	**-0.646**	-0.233	-0.114	**0.563**	**-0.354**	1			
gTurb	**-0.598**	**-0.577**	**-0.315**	**0.695**	**-0.794**	-0.009	1		
gpH	-0.189	0.010	0.001	-0.069	**-0.743**	0.148	0.293	1	
gDist	**0.363**	**0.378**	**0.384**	**-0.505**	**0.483**	**0.394**	**-0.886**	-0.017	1

518

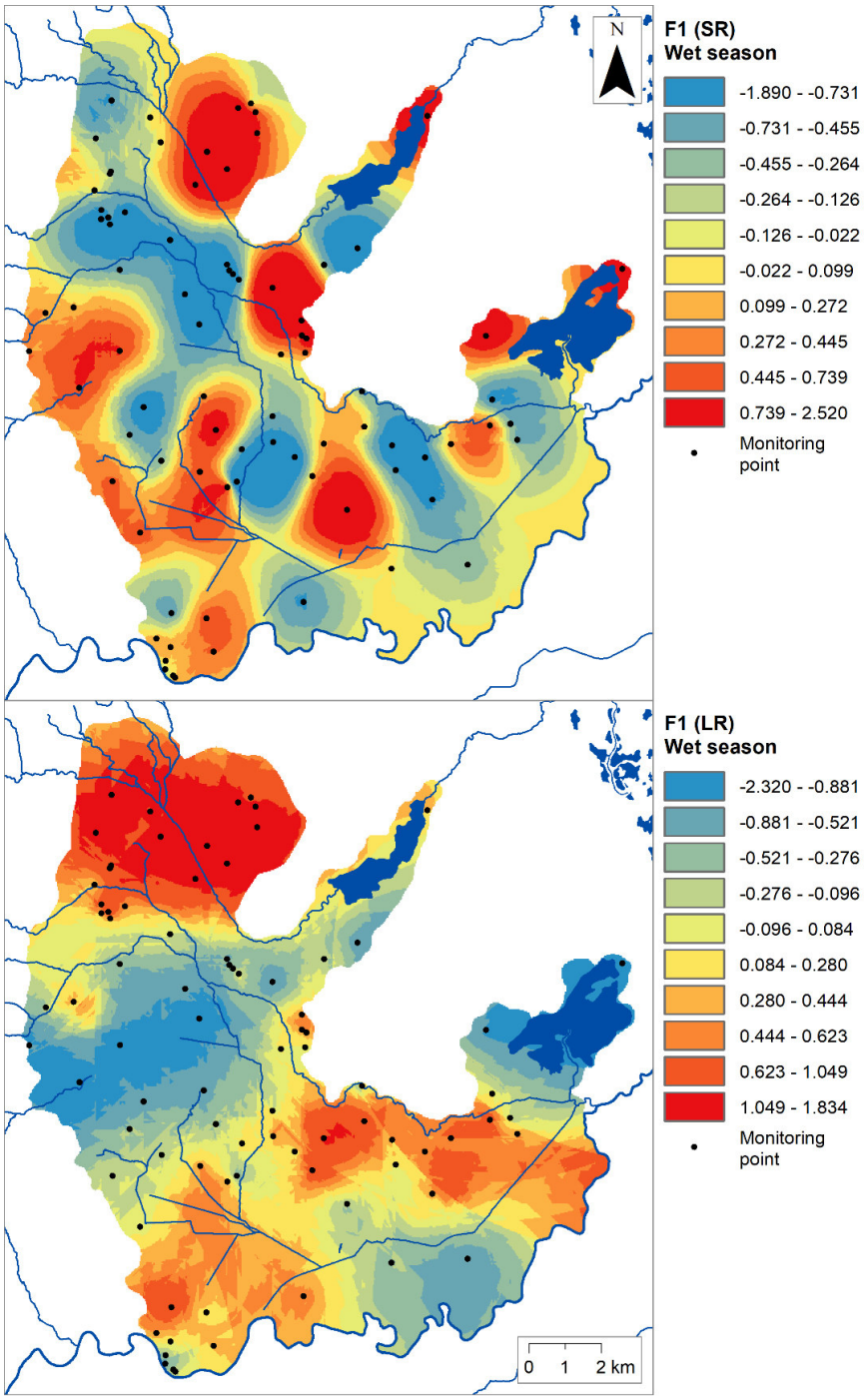

Fig. 7. Maps of the regionalized factor scores, at short (a) and long (b) range. In legend, each class represents one decile (i.e. iso-frequency color scale).

3.6. Conceptual model

The obtained results allowed to define a conceptual model that describes the causes that favor the TEAPs in the San Pedro Sula groundwater (Fig. 8).

In particular, the highly eutrophicated streams in the eastern part of the urban area transfer organic matter into the shallower aquifer layers, since these are hydraulically connected

528 with surface-water. This organic matter, oxidizing, favors anoxic conditions, that cause Mn
529 and Fe oxi-hydroxide reductive dissolution and inhibit the NH_4 oxidation to NO_3^-. The
530 mixed redox conditions in the monitoring wells, where different aquifer layers are present,
531 cause the TEAP regression and Fe oxi-hydroxide precipitation as a colloidal phase.
532 In the northern area, the high Mn and Fe concentrations (Fig. 4), above the WHO
533 thresholds, are related to the organic groundwater contamination likely occurring in the
534 industrial district, that triggers hydrogeochemical changes at the short and long range (Fig.
535 7).
536

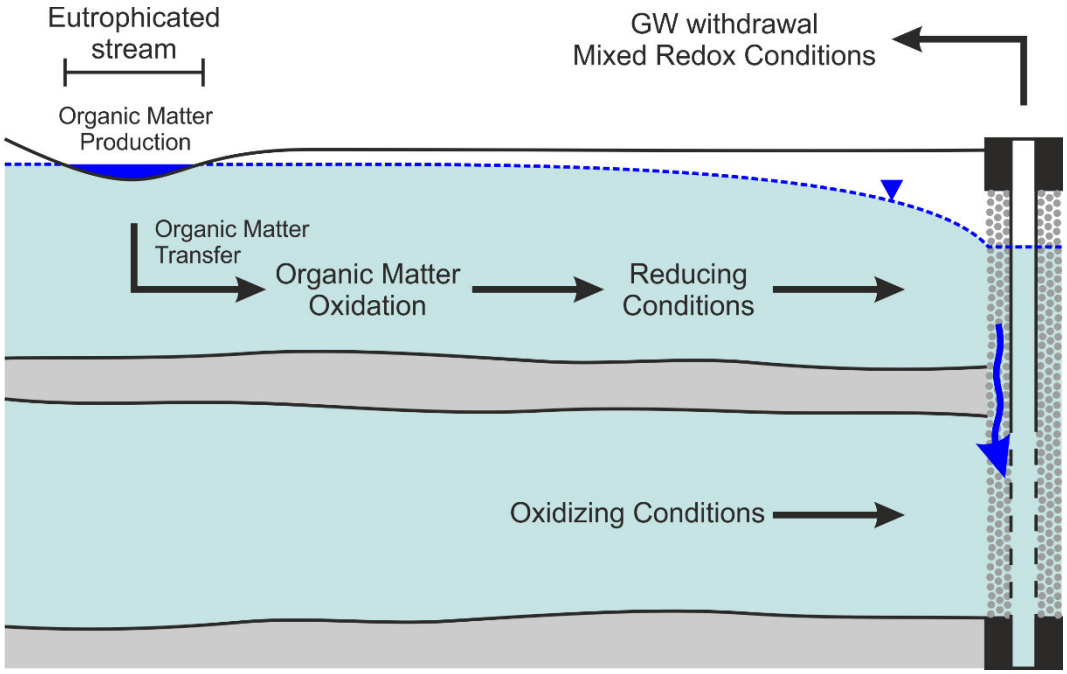

537
538 *Fig. 8. Modello concettuale delle cause dei TEAPs nelle acque sotterranee della piana di San Pedro Sula.*
539

540 **4. Conclusions**

541 The MCFK results, supported by the PCA and hydrogeochemical modeling results,
542 demonstrated that different TEAPs occurring simultaneously in a specific area can be
543 identified.
544 In the San Pedro Sula aquifer, two short-range redox processes (i.e. Mn oxi-hydroxide
545 reductive dissolution and Fe oxi-hydroxide precipitation as a colloidal phase) were

546 identified, related to the organic matter leached from the eutrophicated streams into the
547 shallow aquifer layers, where surface-water/groundwater relationships exist. Furthermore,
548 an additional long-range redox process was detected (i.e. Fe oxi-hydroxide reductive
549 dissolution), related to the organic groundwater contamination likely occurring in the
550 northern area. The obtained information emphasize that there is not a predominant TEAP,
551 but rather a combination of simultaneous redox processes.
552 The individuation of simultaneous redox processes allows overcoming the concepts of
553 predominant TEAPs and homogeneous redox zones, because not completely
554 representative of the actual redox conditions of aquifers, especially when different
555 contamination events occur concomitantly. In addition to identifying all the different TEAPs
556 occurring in the aquifer, the multivariate geostatistical analysis allows discovering, with a
557 certain degree of reliability, the causes that trigger TEAPs in groundwater.
558 In conclusion, the multivariate geostatistical approach used to perform the advanced
559 aquifer redox zonation, i.e. the Multi-Collocated Factorial Kriging, can certainly be
560 implemented in other studies on redox zonation, to obtain a detailed distribution of the
561 TEAPs occurring in a specific aquifer. Furthermore, the proposed method can be used
562 even when detailed information about the contamination, either anthropogenic or natural,
563 as well as its sources, that affects a specific aquifer and triggers anoxic conditions in
564 groundwater, are not clearly determinated.
565

566 **References**

567 Aldrich, M.J., Adams, A.I., Escobar, C., 1991. Structural geology and stress history of the
568 Platanares geothermal site, Honduras: implications on the tectonics of the northwestern
569 Caribbean plate boundary. Journal of Volcanology and Geothermal Research 45, 59–69.
570 doi: 10.1016/0377-0273(91)90022-R

571 Andrade, A.I.A.S.S., Stigter, T.Y., 2013. The distribution of arsenic in shallow alluvial
572 groundwater under agricultural land in central Portugal: Insights from multivariate
573 geostatistical modeling. Science of The Total Environment 449, 37–51. doi:
574 10.1016/j.scitotenv.2013.01.033
575 APHA-AWWA, 1998. Standard methods for the examination of water and wastewater 20.
576 Appelo, C.A.J., Postma, D., 2005. Geochemistry, Groundwater and Pollution. CRC press.
577 Balistrieri, L.S., Seal, R.R., Piatak, N.M., Paul, B., 2007. Assessing the concentration,
578 speciation, and toxicity of dissolved metals during mixing of acid-mine drainage and
579 ambient river water downstream of the Elizabeth Copper Mine, Vermont, USA. Applied
580 Geochemistry 22, 930–952. doi: 10.1016/j.apgeochem.2007.02.005
581 Ball & Nordstrom, 2001
582 Barbieri, M., Carrera, J., Sanchez-Vila, X., Ayora, C., Cama, J., Köck-Schulmeyer, M.,
583 López de Alda, M., Barceló, D., Tobella Brunet, J., Hernández García, M., 2011.
584 Microcosm experiments to control anaerobic redox conditions when studying the fate of
585 organic micropollutants in aquifer material. Journal of Contaminant Hydrology 126, 330–
586 345. doi: 10.1016/j.jconhyd.2011.09.003
587 Berner, R.A., 1981. A New Geochemical Classification of Sedimentary Environments.
588 SEPM Journal of Sedimentary Research 51, 359–365. doi: 10.1306/212F7C7F-2B24-
589 11D7-8648000102C1865D
590 Boano, F., Demaria, A., Revelli, R., Ridolfi, L., 2010. Biogeochemical zonation due to
591 intrameander hyporheic flow. Water Resources Research 46, 1–13. doi:
592 10.1029/2008WR007583
593 Borch, T., Kretzschmar, R., Kappler, A., Cappellen, P. Van, Ginder-Vogel, M., Voegelin,
594 A., Campbell, K., 2010. Biogeochemical Redox Processes and their Impact on
595 Contaminant Dynamics. Environmental Science & Technology 44, 15–23. doi:
596 10.1021/es9026248

597 Buss, H.L., Sak, P.B., Webb, S.M., Brantley, S.L., 2008. Weathering of the Rio Blanco
598 quartz diorite, Luquillo Mountains, Puerto Rico: Coupling oxidation, dissolution, and
599 fracturing. Geochimica et Cosmochimica Acta 72, 4488–4507. doi:
600 10.1016/j.gca.2008.06.020
601 Capaccioni, B., Franco, T., Alberto, R., Orlando, V., Marco, M., Salvatore, I., 2014.
602 Geochemistry of thermal fluids in NW Honduras: New perspectives for exploitation of
603 geothermal areas in the southern Sula graben. Journal of Volcanology and Geothermal
604 Research 280, 40–52. doi: 10.1016/j.jvolgeores.2014.04.004
605 Cary, L., Petelet-Giraud, E., Bertrand, G., Kloppmann, W., Aquilina, L., Martins, V., Hirata,
606 R., Monte-negro, S., Pauwels, H., Chatton, E., Franzen, M., Aurouet, A., Lasseur, E.,
607 Picot, G., Guerrot, C., Fléhoc, C., Labasque, T., Santos, J.G., Paiva, A., Braibant, G.,
608 Pierre, D., 2015. Origins and processes of groundwater salinization in the urban coastal
609 aquifers of Recife (Pernambuco, Brazil): A multi-isotope approach. Science of The Total
610 Environment 530–531, 411–429. doi: 10.1016/j.scitotenv.2015.05.015
611 Castrignanò, A., 2011. Introduction to spatial data processing. ARACNE Editrice.
612 Castrignanò, A., Landrum, C., De Benedetto, D., 2015. Delineation of Management Zones
613 in Precision Agriculture by Integration of Proximal Sensing with Multivariate Geostatistics.
614 Examples of Sensor Data Fusion. Agriculturae Conspectus Scientificus 80, 39–45.
615 Castrignanò, A., Wong, M.T.F., Stelluti, M., De Benedetto, D., Sollitto, D., 2012. Use of
616 EMI, gamma-ray emission and GPS height as multi-sensor data for soil characterisation.
617 Geoderma 175–176, 78–89. doi: 10.1016/j.geoderma.2012.01.013
618 Chapelle, F., Haack, S.K., Adriaens, P., Henry, M.A., Bradley, P.M., 1996. Comparison of
619 Eh and H2 Measurements for Delineating Redox Processes in a Contaminated Aquifer.
620 Environmental Science & Technology 30, 3565–3569. doi: 10.1021/es960249+

621 Chapelle, F.H., Bradley, P.M., Goode, D.J., Tiedeman, C., Lacombe, P.J., Kaiser, K.,
622 Benner, R., 2009a. Biochemical Indicators for the Bioavailability of Organic Carbon in
623 Ground Water. Ground Water 47, 108–121. doi: 10.1111/j.1745-6584.2008.00493.x
624 Chapelle, F.H., Bradley, P.M., Thomas, M.A., McMahon, P.B., 2009b. Distinguishing Iron-
625 Reducing from Sulfate-Reducing Conditions. Ground Water 47, 300–305. doi:
626 10.1111/j.1745-6584.2008.00536.x
627 Chapelle, F.H., O'Neill, K., Bradley, P.M., Methé, B.A., Ciufo, S.A., Knobel, L.L., Lovley,
628 D.R., 2002. A hydrogen-based subsurface microbial community dominated by
629 methanogens. Nature 415, 312–315. doi: 10.1038/415312a
630 Chilès, J.-P., Delfiner, P., 2009. Geostatistics: modeling spatial uncertainty. John Wiley &
631 Sons.
632 Christensen, T.H., Bjerg, P.L., Banwart, S. a, Jakobsen, R., Heron, G., Albrechtsen, H.-J.,
633 2000. Characterization of redox conditions in groundwater contaminant plumes. Journal of
634 Contaminant Hydrology 45, 165–241. doi: 10.1016/S0169-7722(00)00109-1
635 Close, M.E., Abraham, P., Humphries, B., Lilburne, L., Cuthill, T., Wilson, S., 2016.
636 Predicting groundwater redox status on a regional scale using linear discriminant analysis.
637 Journal of Contaminant Hydrology 191, 19–32. doi: 10.1016/j.jconhyd.2016.04.006
638 Desiderio, G., Rusi, S., Tatangelo, F., 2010. Caratterizzazione idrogeochimica delle acque
639 sotterranee abruzzesi e relative anomalie. Italian Journal of Geosciences 129, 207–222.
640 doi: 10.3301/IJG.2010.05
641 Dessert, C., Dupré, B., Gaillardet, J., François, L.M., Allègre, C.J., 2003. Basalt weathering
642 laws and the impact of basalt weathering on the global carbon cycle. Chemical Geology
643 202, 257–273. doi: 10.1016/j.chemgeo.2002.10.001
644 Di Curzio, D., Palmucci, W., Rusi, S., Signanini, P., 2016. Evaluation of processes
645 controlling Fe and Mn contamination in the San Pedro Sula porous aquifer (North Western

646 Honduras). Rendiconti Online della Società Geologica Italiana 41, 42–45. doi:
647 10.3301/ROL.2016.88
648 Di Curzio, D., Rusi, S., Semeraro, R., 2018. Multi-scenario numerical modeling applied to
649 groundwater contamination: the Popoli Gorges complex aquifer case study (Central Italy)
650 Italian Journal of Groundwater 7, 4/154, 49-58, doi: 10.7343/as-2018-361 Donnelly, T.W.,
651 Horne, G.S., Finch, R.C., Lopez-Ramos, E., 1990. Northern Central America; the Maya
652 and Chortis blocks. The Geology of North America 11, 37–76.
653 Druschel, G.K., Emerson, D., Sutka, R., Suchecki, P., Luther, G.W., 2008. Low-oxygen
654 and chemical kinetic constraints on the geochemical niche of neutrophilic iron(II) oxidizing
655 microorganisms. Geochimica et Cosmochimica Acta 72, 3358–3370. doi:
656 10.1016/j.gca.2008.04.035
657 Du, C., Liu, E., Chen, N., Wang, W., Gui, Z., He, X., 2017. Factorial kriging analysis and
658 pollution evaluation of potentially toxic elements in soils in a phosphorus-rich area, South
659 Central China. Journal of Geochemical Exploration 175, 138–147. doi:
660 10.1016/j.gexplo.2017.01.010
661 Ducci, D., de Melo, M.T.C., Preziosi, E., Sellerino, M., Parrone, D., Ribeiro, L., 2016.
662 Combining natural background levels (NBLs) assessment with indicator kriging analysis to
663 improve groundwater quality data interpretation and management. Science of The Total
664 Environment 569–570, 569–584. doi: 10.1016/j.scitotenv.2016.06.184
665 Finch, R.C., 1981. Mesozoic stratigraphy of central Honduras. AAPG Bulletin 65, 1320–
666 1333.
667 Gaillardet, J., Dupré, B., Louvat, P., Allègre, C.J., 1999. Global silicate weathering and
668 CO2 consumption rates deduced from the chemistry of large rivers. Chemical Geology
669 159, 3–30. doi: 10.1016/S0009-2541(99)00031-5
670 Garza, R.S.M., van Hinsbergen, D.J.J., Rogers, R.D., Ganerød, M., Dekkers, M.J., 2012.
671 The Padre Miguel Ignimbrite Suite, central Honduras: Paleomagnetism, geochronology,

672 and tectonic implications. Tectonophysics 574–575, 144–157. doi:
673 10.1016/j.tecto.2012.08.013
674 Geovariances, 2017. ISATIS software: technical references release 2017.1. Geovariances
675 and Ecole des Mines de Paris, Avon/Fontainebleau.
676 Greskowiak, J., Prommer, H., Massmann, G., Nützmann, G., 2006. Modeling Seasonal
677 Redox Dynamics and the Corresponding Fate of the Pharmaceutical Residue Phenazone
678 During Artificial Re-charge of Groundwater. Environmental Science & Technology 40,
679 6615–6621. doi: 10.1021/es052506t
680 Halim, C.E., Short, S.A., Scott, J.A., Amal, R., Low, G., 2005. Modelling the leaching of Pb,
681 Cd, As, and Cr from cementitious waste using PHREEQC. Journal of Hazardous Materials
682 125, 45–61. doi: 10.1016/j.jhazmat.2005.05.046
683 Heimann, A., Jakobsen, R., Blodau, C., 2010. Energetic Constraints on H 2 -Dependent
684 Terminal Electron Accepting Processes in Anoxic Environments: A Review of
685 Observations and Model Approaches. Environmental Science & Technology 44, 24–33.
686 doi: 10.1021/es9018207
687 Hotelling, H., 1933. Analysis of a complex of statistical variables into principal components.
688 Journal of Educational Psychology 24, 417–441. doi: 10.1037/h0071325
689 Hsu, C.-H., Han, S.-T., Kao, Y.-H., Liu, C.-W., 2010. Redox characteristics and zonation of
690 arsenic-affected multi-layers aquifers in the Choushui River alluvial fan, Taiwan. Journal of
691 Hydrology 391, 351–366. doi: 10.1016/j.jhydrol.2010.07.037
692 Hunter, K.S., Wang, Y., Van Cappellen, P., 1998. Kinetic modeling of microbially-driven
693 redox chemistry of subsurface environments: coupling transport, microbial metabolism and
694 geochemistry. Journal of Hydrology 209, 53–80. doi: 10.1016/S0022-1694(98)00157-7
695 Islam, F.S., Gault, A.G., Boothman, C., Polya, D.A., Charnock, J.M., Chatterjee, D., Lloyd,
696 J.R., 2004. Role of metal-reducing bacteria in arsenic release from Bengal delta
697 sediments. Nature 430, 68–71. doi: 10.1038/nature02638

698 Jackson, B.E., McInerney, M.J., 2002. Anaerobic microbial metabolism can proceed close
699 to thermodynamic limits. Nature 415, 454–456. doi: 10.1038/415454a
700 Jakobsen, R., Cold, L., 2007. Geochemistry at the sulfate reduction–methanogenesis
701 transition zone in an anoxic aquifer—A partial equilibrium interpretation using 2D reactive
702 transport modeling. Geochimica et Cosmochimica Acta 71, 1949–1966. doi:
703 10.1016/j.gca.2007.01.013
704 Kloppmann, W., Dever, L., Edmunds, W.M., 1996. Zones d'oxydo-réduction dans
705 l'aquifère de la Craie des bassins de Paris et de l'Allemagne du nord. Hydrological
706 Sciences Journal 41, 311–326. doi: 10.1080/02626669609491505
707 Kotaś, J., Stasicka, Z., 2000. Chromium occurrence in the environment and methods of its
708 speciation. Environmental Pollution 107, 263–283. doi: 10.1016/S0269-7491(99)00168-2
709 Landon, M.K., Green, C.T., Belitz, K., Singleton, M.J., Esser, B.K., 2011. Relations of
710 hydrogeologic factors, groundwater reduction-oxidation conditions, and temporal and
711 spatial distributions of ni-trate, Central-Eastside San Joaquin Valley, California, USA.
712 Hydrogeology Journal 19, 1203–1224. doi: 10.1007/s10040-011-0750-1
713 Lee, A.., Nikraz, H., 2015. BOD: COD Ratio as an Indicator for River Pollution.
714 International Proceedings of Chemical, Biological and Environmental Engineering, 51,
715 139–142. doi: 10.7763/IPCBEE.
716 Lewandowski, J., Meinikmann, K., Nützmann, G., Rosenberry, D.O., 2015. Groundwater -
717 the disregarded component in lake water and nutrient budgets. Part 2: effects of
718 groundwater on nutrients. Hydrological Processes 29, 2922–2955. doi: 10.1002/hyp.10384
719 Lin, C.Y., Abdullah, M.H., Praveena, S.M., Yahaya, A.H.B., Musta, B., 2012. Delineation of
720 temporal variability and governing factors influencing the spatial variability of shallow
721 groundwater chemistry in a tropical sedimentary island. Journal of Hydrology 432–433,
722 26–42. doi: 10.1016/j.jhydrol.2012.02.015

723 Lønborg, M.J., Engesgaard, P., Bjerg, P.L., Rosbjerg, D., 2006. A steady state redox zone
724 approach for modeling the transport and degradation of xenobiotic organic compounds
725 from a landfill site. Journal of Contaminant Hydrology 87, 191–210. doi:
726 10.1016/j.jconhyd.2006.05.004
727 Madonna, R., Torrese, P., Crema, G., Signanini, P., Costantino, V., 2007. Composizione
728 delle rocce e qualità delle acque nell'area di San Pedro Sula (Honduras) [Rocks
729 composition and water quality of San Pedro Sula area (Honduras)]. Italian Journal of
730 Engineering Geology and Environment 1, 19–32.
731 Matheron, G., 1982. Pour une analyse krigeante des données regionalisées in Report 732.
732 Centre de Geostatistique, Fontainebleau.
733 McCarty, P.L., 1997. Breathing with Chlorinated Solvents. Science 276, 1521–1522. doi:
734 10.1126/science.276.5318.1521
735 McMahon, P.B., Chapelle, F.H., 1991. Microbial production of organic acids in aquitard
736 sediments and its role in aquifer geochemistry. Nature 349, 233–235. doi:
737 10.1038/349233a0
738 McMahon, P.B., Chapelle, F.H., 2008. Redox Processes and Water Quality of Selected
739 Principal Aquifer Systems. Ground Water 46, 259–271. doi: 10.1111/j.1745-
740 6584.2007.00385.x
741 Meinikmann, K., Hupfer, M., Lewandowski, J., 2015. Phosphorus in groundwater
742 discharge – A potential source for lake eutrophication. Journal of Hydrology 524, 214–226.
743 doi: 10.1016/j.jhydrol.2015.02.031
744 Meneses, B.M., Reis, R., Vale, M.J., Saraiva, R., 2015. Land use and land cover changes
745 in Zêzere watershed (Portugal) — Water quality implications. Science of The Total
746 Environment 527–528, 439–447. doi: 10.1016/j.scitotenv.2015.04.092
747 Molinari, A., Ayora, C., Marcaccio, M., Guadagnini, L., Sanchez-Vila, X., Guadagnini, A.,
748 2014. Geochemical modeling of arsenic release from a deep natural solid matrix under

749 alternated redox conditions. Environmental Science and Pollution Research 21, 1628–
750 1637. doi: 10.1007/s11356-013-2054-6
751 Nedrich, S.M., Chappaz, A., Hudson, M.L., Brown, S.S., Burton, G.A., 2018.
752 Biogeochemical controls on the speciation and aquatic toxicity of vanadium and other
753 metals in sediments from a river reservoir. Science of The Total Environment 612, 313–
754 320. doi: 10.1016/j.scitotenv.2017.08.141
755 Palmucci, W., Rusi, S., 2014. Boron-rich groundwater in Central Eastern Italy: a
756 hydrogeochemical and statistical approach to define origin and distribution. Environmental
757 Earth Sciences 72, 5139–5157. doi: 10.1007/s12665-014-3384-5
758 Palmucci, W., Rusi, S., Di Curzio, D., 2016a. Mobilisation processes responsible for iron
759 and manganese contamination of groundwater in Central Adriatic Italy. Environmental
760 Science and Pollution Research 23, 11790–11805. doi: 10.1007/s11356-016-6371-4
761 Palmucci, W., Rusi, S., Tatangelo, F., 2016b. Ring maps applied to hydrogeological and
762 environmental studies in alluvial aquifers, central Italy, Journal of Maps, 12:1, 33-44. doi:
763 10.1080/17445647.2014.977973
764 Postma, D., Jakobsen, R., 1996. Redox zonation: Equilibrium constraints on the
765 Fe(III)/SO4-reduction interface. Geochimica et Cosmochimica Acta 60, 3169–3175. doi:
766 10.1016/0016-7037(96)00156-1
767 Purcell, J.W., Lovelace, F.D., Girty, G.H., 2015. Biotite controlled chemical alteration of
768 granodioritic–tonalitic saprock: Exploring the use of sieving to enhance compositional
769 linear trends. Geoderma 253–254, 90–101. doi: 10.1016/j.geoderma.2015.04.011
770 Rahnemaie et al., 2007
771 Reeder, R.J., Schoonen, M.A.A., Lanzirotti, A., 2006. Metal Speciation and Its Role in
772 Bioaccessibility and Bioavailability. Reviews in Mineralogy and Geochemistry 64, 59–113.
773 doi: 10.2138/rmg.2006.64.3

774 Rogers, R.D., Mann, P., Emmet, P.A., 2007. Tectonic terranes of the Chortis block based
775 on integration of regional aeromagnetic and geologic data, in: Special Paper 428: Geologic
776 and Tectonic Development of the Caribbean Plate Boundary in Northern Central America.
777 Geological Society of America, pp. 65–88. doi: 10.1130/2007.2428(04)
778 Root, R.A., Vlassopoulos, D., Rivera, N.A., Rafferty, M.T., Andrews, C., O'Day, P.A., 2009.
779 Speciation and natural attenuation of arsenic and iron in a tidally influenced shallow
780 aquifer. Geochimica et Cosmochimica Acta 73, 5528–5553. doi:
781 10.1016/j.gca.2009.06.025
782 Rotiroti, M., Jakobsen, R., Fumagalli, L., Bonomi, T., 2015. Arsenic release and
783 attenuation in a multi-layer aquifer in the Po Plain (northern Italy): Reactive transport
784 modeling. Applied Geochemistry 63, 599–609. doi: 10.1016/j.apgeochem.2015.07.001
785 Rotiroti, M., Sacchi, E., Fumagalli, L., Bonomi, T., 2014. Origin of Arsenic in Groundwater
786 from the Multilayer Aquifer in Cremona (Northern Italy). Environmental Science &
787 Technology 48, 5395–5403. doi: 10.1021/es405805v
788 Rotiroti et al, 2018
789 Rusi, S., Di Curzio, D., Palmucci, W., Petaccia, R., 2018. Detection of the natural origin
790 hydrocarbon contamination in carbonate aquifers (Central Apennine, Italy). Environmental
791 Science and Pollution Research 25, 15577-15596. doi: 10.1007/s11356-018-1769-9Ryan,
792 P.C., West, D.P., Hattori, K., Studwell, S., Allen, D.N., Kim, J., 2015. The influence of
793 meta-morphic grade on arsenic in metasedimentary bedrock aquifers: A case study from
794 Western New England, USA. Science of The Total Environment 505, 1320–1330. doi:
795 10.1016/j.scitotenv.2014.05.021
796 Skubal, K.L., Haack, S.K., Forney, L.J., Adriaens, P., 1999. Effects of dynamic redox
797 zonation on the potential for natural attenuation of trichloroethylene at a fire-training-
798 impacted aquifer. Physics and Chemistry of the Earth, Part B: Hydrology, Oceans and
799 Atmosphere 24, 517–527. doi: 10.1016/S1464-1909(99)00039-8

800 Sollitto, D., Romic, M., Castrignanò, A., Romic, D., Bakic, H., 2010. Assessing heavy metal
801 contamination in soils of the Zagreb region (Northwest Croatia) using multivariate
802 geostatistics. Catena 80, 182–194. doi: 10.1016/j.catena.2009.11.005
803 Sracek, O., Bhattacharya, P., Jacks, G., Gustafsson, J., Brömssen, M. von, 2004.
804 Behavior of arsenic and geochemical modeling of arsenic enrichment in aqueous
805 environments. Applied Geochemistry 19, 169–180. doi: 10.1016/j.apgeochem.2003.09.005
806 Torrese, P., Madonna, R., Signanini, P., Costantino, V., 2006. Modellazione dell'acquifero
807 sub-tropicale della città di San Pedro Sula (Honduras) finalizzata alla gestione della risorsa
808 idrica [Hydrodynamic numerical model aimed to water management and withdrawal of
809 sub-tropical allu-vial aquifer in San Pedro Sula area. Italian Journal of Engineering
810 Geology and Environment 2, 23–41.
811 Torrese, P., Rainone, M.L., Colantonio, F., Signanini, P., 2013. Identification and
812 investigation of shallow paleochannels in the Chamelecon valley (Honduras): 1D vs 2D
813 electrical resistivity surveys. 26th Symposium on the Application of Geophysics to
814 Engineering and Environmental Problems 2013, SAGEEP 2013.
815 Vessia & Di Curzio 2018
816 Viaroli, S., Cuoco, E., Mazza, R., Tedesco, D., 2016. Dynamics of natural contamination
817 by aluminium and iron rich colloids in the volcanic aquifers of Central Italy. Environmental
818 Science and Pollu-tion Research 23, 19958–19977. doi: 10.1007/s11356-016-7198-8
819 Wackernagel, H., 2003. Multivariate Geostatistics: An Introduction with Applications.
820 Springer-Verlag, Berlin.
821 Wallis, I., Prommer, H., Simmons, C.T., Post, V., Stuyfzand, P.J., 2010. Evaluation of
822 Conceptual and Numerical Models for Arsenic Mobilization and Attenuation during
823 Managed Aquifer Re-charge. Environmental Science & Technology 44, 5035–5041. doi:
824 10.1021/es100463q

825 Wang, L., Xu, S., Li, J., 2011. Effects of Phosphate on the Transport of Escherichia coli
826 O157:H7 in Saturated Quartz Sand. Environmental Science & Technology 45, 9566–9573.
827 doi: 10.1021/es201132s
828 Watson, I.A., Oswald, S.E., Mayer, K.U., Wu, Y., Banwart, S.A., 2003. Modeling Kinetic
829 Processes Controlling Hydrogen and Acetate Concentrations in an Aquifer-Derived
830 Microcosm. Environmental Science & Technology 37, 3910–3919. doi:
831 10.1021/es020242u
832 Webster, R., Oliver, M.A., 2007. Geostatistics for Environmental Scientists. John Wiley &
833 Sons.
834 WHO, 2011. Guidelines for Drinking-water Quality. WHO Library Cataloguing-in-
835 Publication Data. Available at:
836 http://www.who.int/water_sanitation_health/publications/2011/dwq_guidelines/en/